High Density Polyethylene/Polystyrene Blends: Phase Distribution Morphology, Rheological Measurements, Extrusion, and Melt Spinning Behavior

KYONSUKU MIN, JAMES L. WHITE,* and JOHN F. FELLERS,
Polymer Engineering, University of Tennessee, Knoxville, Tennessee 37996

Synopsis

An experimental study of the development of phase morphology, rheological properties, and processing behavior of mechanical blends of a polystyrene (PS) and a high density polyethylene (PE) is presented. Phase morphologies were determined by scanning electron microscopy for (i) products prepared in a screw extruder/static mixer system, (ii) samples removed from a cone-plate viscometer, (iii) extrudates, and (iv) melt spun fibers. Disperse phase dimensions were measured. The values varied from 1–5 μm in the products from static mixers. The dimensions of the dispersed phase in the blend products from the cone plate and capillary die were of the same order. The melt-spun fibers exhibited disperse phase dimensions as low as 0.35 μm. Polystyrene was extracted from the blend fibers producing small diameter, PE fibrils, or minifibers. Both the initial melts and the blends were rheologically characterized. The shear viscosity and principal normal stress difference N_1 exhibit maxima and minima when plotted as a function of composition. The characteristics of extrudates and melt spinning behavior of the blends were investigated. The shrinkage of extrudates of PE is much greater than PS. Additional small amounts of PE to PS greatly increase its shrinkage. Addition of PE to PS initially increases extrudate swell, though the swell shows maxima and minima when considered as a function of composition. The positions of the maxima and minima correspond to those of N_1. The onset of draw resonance has been investigated in isothermal melt spinning. Wide angle X-ray diffraction studies have been carried out on blend fibers and the orientation of the crystalline polyethylene regions has been determined as a function of process conditions. This orientation decreases rapidly with the addition of polystyrene when the melt-spun filaments are compared at the same spinline stress or drawdown ratio.

INTRODUCTION

Blends of thermoplastics play an increasingly important role in commerce. Fundamental investigations of the influence of mixing and fabrication methods on the phase morphology of blends and the characteristics of the individual phases are of great importance. Basic studies of the morphology and properties of blends require pairs of polymer systems which are readily available in quantity, in a range of molecular weights, are chemically stable and easily distinguishable. No blend system better fills the description than polyethylene–polystyrene. Not surprisingly, this has been the most thoroughly investigated of all polymer blend systems.[1–6] There have also been studies of ternary systems including styrene–ethylene block and graft copolymers.[7–11]

* Present address: Polymer Engineering Center, University of Akron, Akron, Ohio 44325.

Journal of Applied Polymer Science, Vol. 29, 2117–2142 (1984)
 CCC 0021-8995/84/062117-26$04.0(

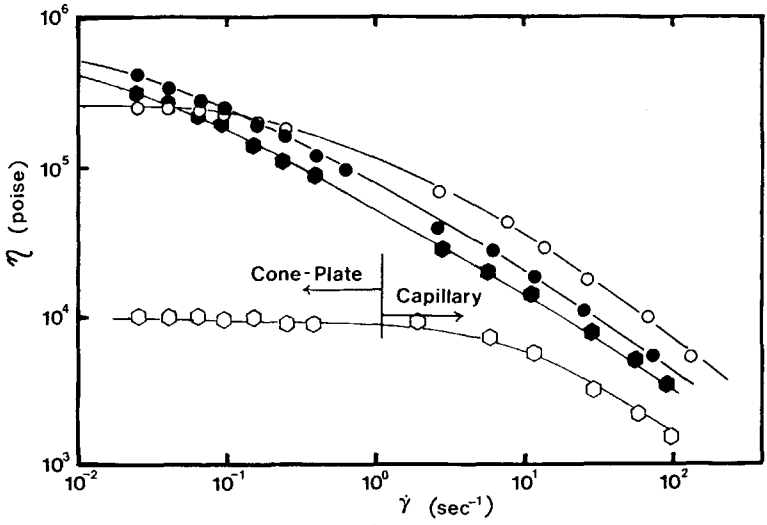

(a)

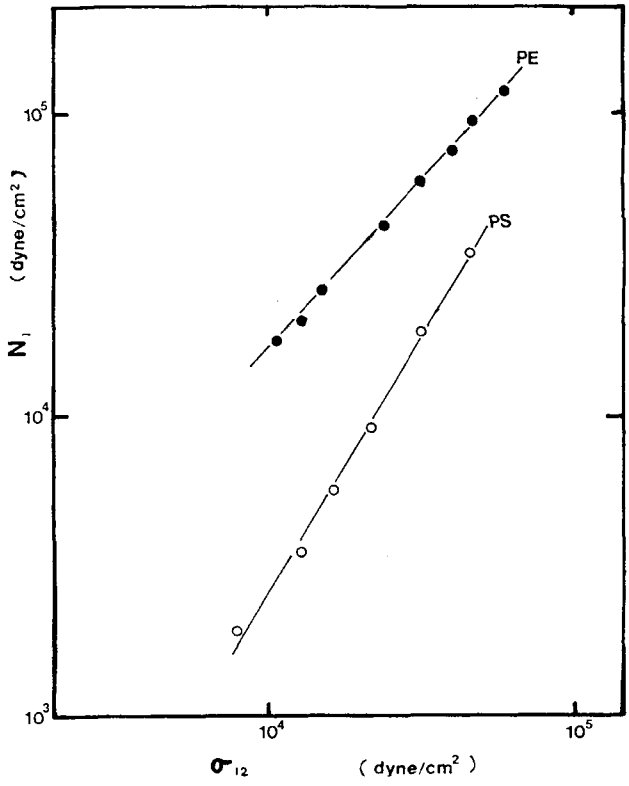

(b)

Fig. 1. (a) Shear viscosity η of PE and PS as a function of shear rate $\dot{\gamma}$ at 180°C and 240°C. PS: (○) 180°C; (○) 240°C; PE: (●) 180°C; (●) 240°C. (b) Principal normal stress difference N_1 as a function of shear stress σ_{12} obtained at 180°C. PE (CX 6109)/PS, 180°C.

The above-cited studies of the polystyrene–polyethylene system tend to be narrow generally emphasizing rheological properties,[1,3,4] phase morphology,[5,8–10] mechanical properties[2,5,7,10,11] or some combination of the latter two topics. What is lacking are integrated studies including (i) rheological properties of the

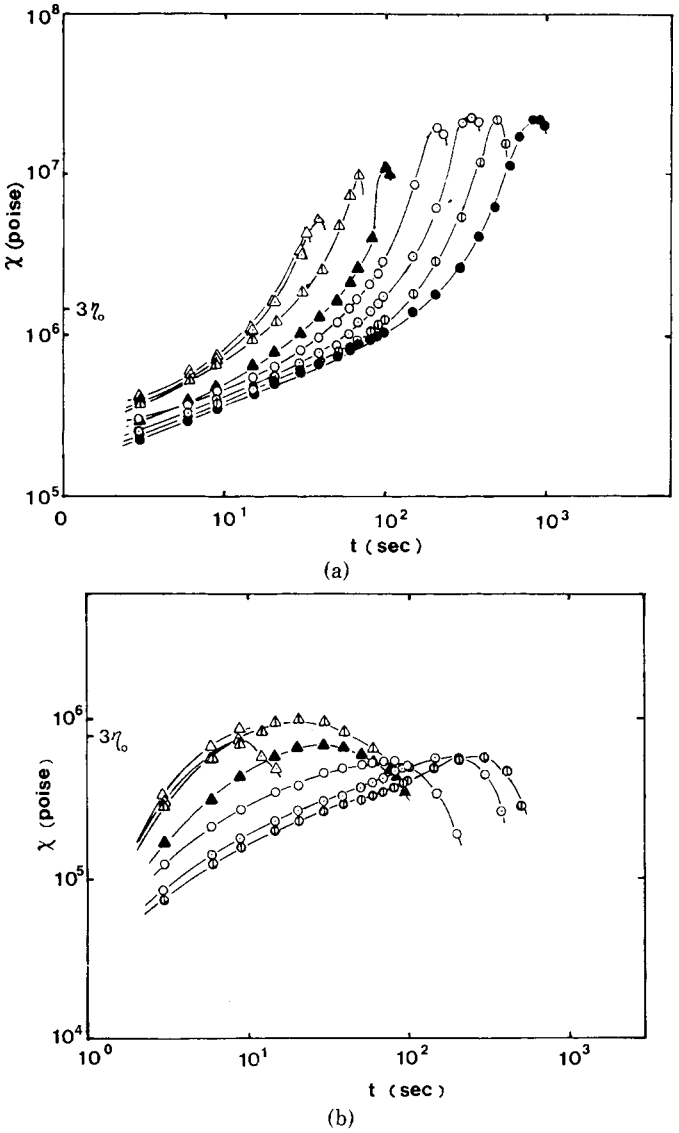

Fig. 2. Elongational viscosity χ as a function of stretch rate and time for (a) PE (CX 6109) and (b) PS (180°C) E (s^{-1}): (a) (●) 4.46×10^{-3}; (Φ) 7.14; (⊙) 1.22×10^{-2}; (○) 1.95; (▲) 3.31; (▲) 5.60; (▲) 9.10; (△) 1.50×10^{-1}; (b) (Φ) 7.14×10^{-3}; (⊙) 1.22×10^{-2}; (○) 1.95×10^{-2}; (▲) 3.31×10^{-2}; (▲) 5.60×10^{-2}; (▲) 9.10×10^{-2}; (△) 1.50×10^{-1}.

individual components, (ii) phase morphology of blends as a function of process history, (iii) rheological properties of the blends, and (iv) processing characteristics of the blends. We present such a study in this paper. We include an investigation of the melt spinning of the blend systems including spinline stability, development of polymer chain orientation in the polyethylene phase, and the formation of small diameter minifilaments.

EXPERIMENTAL

Materials. The polymers included in this study are a commercial high density polyethylene (PE) (Chemplex 6109, MI = 0.9) and a commercial polystyrene (PS) (Dow Styron 678U).

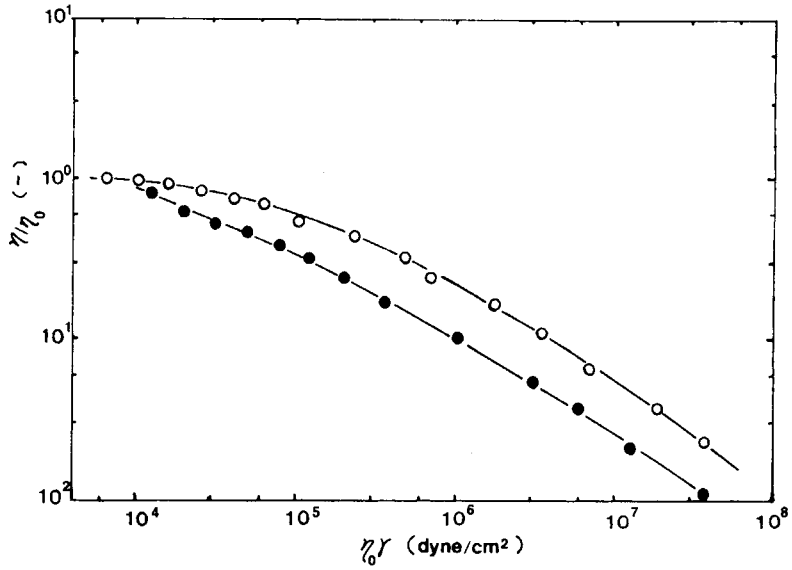

Fig. 3. Reduced viscosity η/η_0 as a function of $\eta_0\dot{\gamma}$ for PE (CX 6109) (●) and PS (○).

Blending. Blends with compositions of 90/10, 70/30, 50/50, 30/70, 10/90 were prepared with a 0.75-in. Brabender screw extruder with a KMB-100 Koch static mixer with four elements at both 180°C and 240°C. The extruder screw rotated at 35 rpm.

Scanning Electron Microscopy. The phase morphologies were determined using an AMR high resolution scanning electron microscope. Fracture surfaces were prepared in liquid nitrogen. In many studies, the polystyrene was extracted with toluene leaving a polyethylene residue. The polymer samples were coated with a gold–palladium alloy before viewing.

Rheological Properties. The shear viscosity and principal normal stress difference of the PS, PE, and their blends were measured in a rheometrics mechanical spectrometer, in the cone-plate mode. The shear rate in this instrument is

$$\dot{\gamma} = \Omega/\alpha \tag{1}$$

where Ω is the angular velocity and α is the cone angle. The shear stress σ_{12} and principal normal stress difference N_1 are given by[12,13]

$$\sigma_{12} = 3M/2\pi R^3 \tag{2a}$$

$$N_1 = 2F/\pi R^2 \tag{2b}$$

where M is the torque, F is the thrust, and R is the cone radius. In our studies a cone radius of 2.5 cm and a cone angle of 0.1 rad were used. At higher shear rates, shear viscosities were determined in a Merz–Colwell Instron capillary rheometer. The shear stress on the die wall $(\sigma_{12})_w$ is related to the total pressure p_T, pushing melt through the die. This is expressed by[12,13]

$$p_T = 4(\sigma_{12})_w L/D + \Delta p_{\text{ends}} \tag{3}$$

where L is the length and D the diameter of the die. Δp_{ends} is the (ends) pressure loss. $(\sigma_{12})_w$ is determined from a plot of p_T vs. L/D. Dies of diameter 0.058 in. and L/D ratios of 10, 20, 30, and 40 were used.

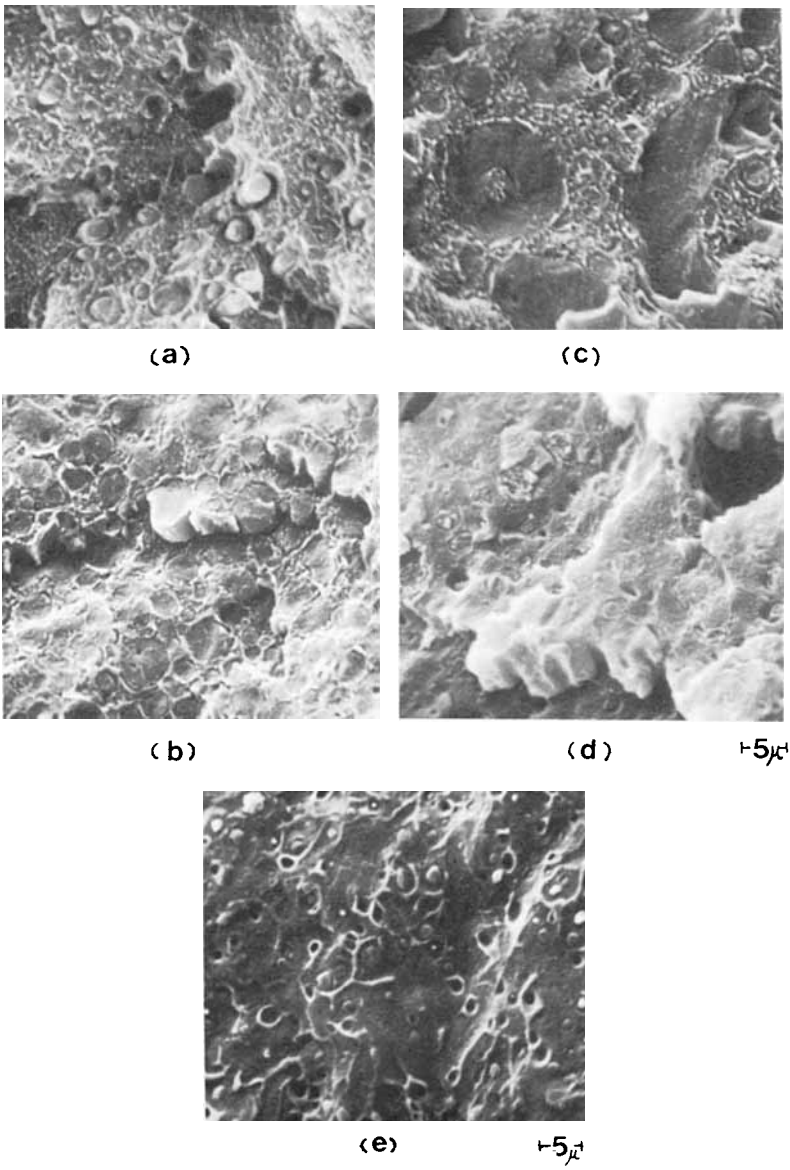

Fig. 4. SEM phase morphology of fracture surfaces of PE/PS blends mixed in a screw extruder–static mixer in combination at 180°C: (a) 90/10; (b) 70/30; (c) 50/50; (d) 30/70; (e) 10/90.

Elongational viscosities of the blends were measured in an instrument developed in our laboratories and described in a series of papers from our laboratories.[14–16]

Extrudate Shrinkage. Extrudates were prepared from the Brabender extruder which had a capillary die. These were placed in a hot silicone oil bath at 180°C and equilibrated.

Extrudate Swell. The diameters d of extrudates emerging from dies in the Merz–Colwell Instrom capillary rheometer was measured and extrudate swell d/D or B computed. Extrudates emerging from dies were cut at distances of 5 cm below the die exit. Density corrections were made on extrudate swell data to the temperature of the melt in the die.

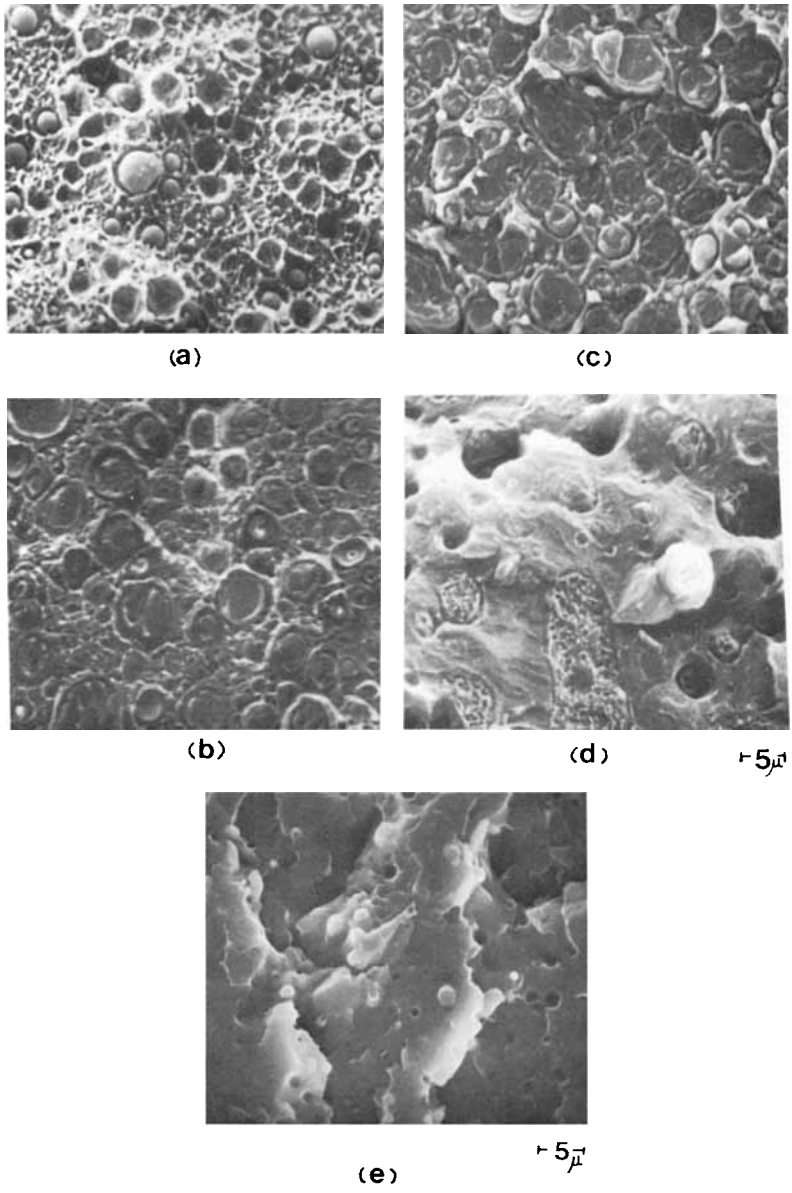

Fig. 5. SEM phase morphology of fracture surfaces for PE/PS blends mixed in a screw extruder–static mixer combination at 240°C: (a) 90/10; (b) 70/30; (c) 50/50; (d) 30/70; (e) 10/90.

Melt Spinning. The blend extrudates were melt-spun from this Instron capillary rheometer through a quench bath and onto a takeup roll as described in earlier papers from our laboratories.[17] A die of diameter 1.5 mm (0.058 in.) and L/D ratio of 40 was used. Drawdown ratios V_L/V_0 up to 215 were prepared tensions were sensed with a Rothschild tensiometer.

We have also investigated filament uniformity and the onset of draw resonance. In these studies an isothermal chamber was placed on the spinline.[17]

Wide Angle X-Ray Diffraction. Wide angle X-ray diffraction studies of blend fibers were carried out using Nickel filtered CuKα radiation.

The PE crystallizes to form an orthorhombic unit cell as first shown by Bunn.[18]

TABLE I
Phase Morphology of PE/PS Blends from Static Mixer

PE/PS composition	Authors' dispersed phase dimensions a_n (μm) 180°C	a_n (μm) 240°C	a_w (μm) 180°C	a_w (μm) 240°C	a_w (μm) Han and Kim[3] 200°C	Han and Kim[3] 240°C	a_w (μm) Barentsen and Heikens[2] 150°C
10/90	1.3	1.8	1.4	2.6	—		1.5
30/70	2.0	3.4	2.6	5.4	7.0	5.6	35
50/50	5.8	3.7	9.2	4.4	6.2	5.1	Cocontinuous
70/30	3.4	3.2	3.9	3.6	Cocontinuous		8.0
90/10	2.9	2.2	2.5	3.0	—		2.5

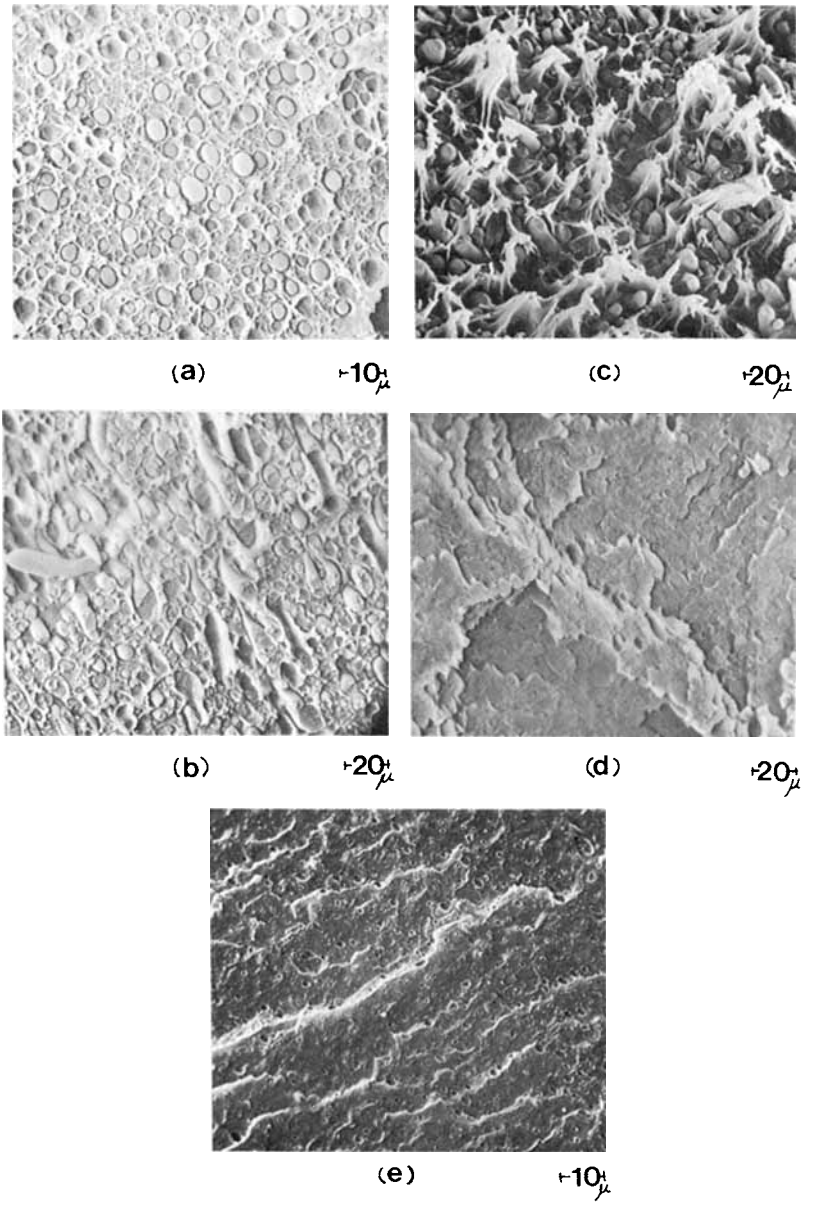

Fig. 6. SEM fracture surfaces of PE/PS samples removed from cone-plate instrument: (a) 90/10; (b) 70/30; (c) 50/50; (d) 30/70; (e) 10/90. T = 180°C.

TABLE II
Phase Morphology of PE/PS Blends from Cone-Plate Gap

PE/PS composition	$\dot{\gamma}$ (s^{-1})	$\sigma_{12} \times 10^{-4}$ (dyn/cm^2)	Dispersed phase a_n (μm)	a_w (μm)
10/90	0.063	2.52	1.4	1.6
30/70	0.1	2.64	4.3	5.0
50/50	0.1	2.71	4.9	5.4
70/30	0.1	2.68	5.6	6.0
90/10	0.1	2.46	2.5	2.3

The uniaxial orientation of PE may be expressed in terms of the Hermans–Stein orientation factors for the three crystallographic axes.[19] These are defined as

$$f_j = (\overline{3 \cos^2} \phi_{1j} - 1)/2 \tag{4}$$

where subscript j refers to the j-crystallographic axis. ϕ_{1j} is the angle between j-axis and the fiber axis. For an orthorhombic unit cell, f_a, f_b, and f_c are interrelated through the Pythagorean theorem. Specifically,

$$f_a + f_b + f_c = 0 \tag{5}$$

The strongest WAXS reflections for polyethylene are the 110, 200, and 020 reflections. The 200 may be used to obtain f_a. The orientation factor f_b was obtained using Stein's expression[19] from the 110 and 200 reflections

$$\cos^2 \phi_{1b} = \frac{\cos^2 \phi_{110,1} - 0.308 \cos^2 \phi_{200,1}}{0.692} \tag{6}$$

f_c was determined from eq. (5).

Formation of Minifibers. Blend filaments containing 10% PE and 90% PS were extracted in toluene. This removed the PS and left behind a PE residue generally in the form of small diameter (mini) filaments.

TABLE III
Phase Morphology of PE/PS Blend from Capillary Die

Composition PE/PS	$\dot{\gamma}_w$ (s^{-1})	$(\sigma_{12})_w$ (dyn/cm^2)	a_n (μm)	a_w (μm)
90/10	2.13	1.02×10^5	1.94	2.13
	11.5	2.60	1.29	1.38
	64.8	4.80	1.17	1.33
30/70	2.26	0.94×10^5	3.33	4.27
	12.26	2.75	2.46	2.96
70/30	69.6	5.70	2.19	2.45
50/50	2.02	0.94×10^5	3.72	4.25
	11.04	2.20	2.65	3.02
	70.8	4.68	2.30	2.71
30/70	2.21	1.56×10^5	1.70	1.85
	12.24	3.12	1.44	1.52
	52.8	5.00	0.87	1.18
10/90	2.59	2.50×10^5	1.59	1.72
	13.9	3.90	0.70	0.91
	60.0	7.03	0.44	0.53

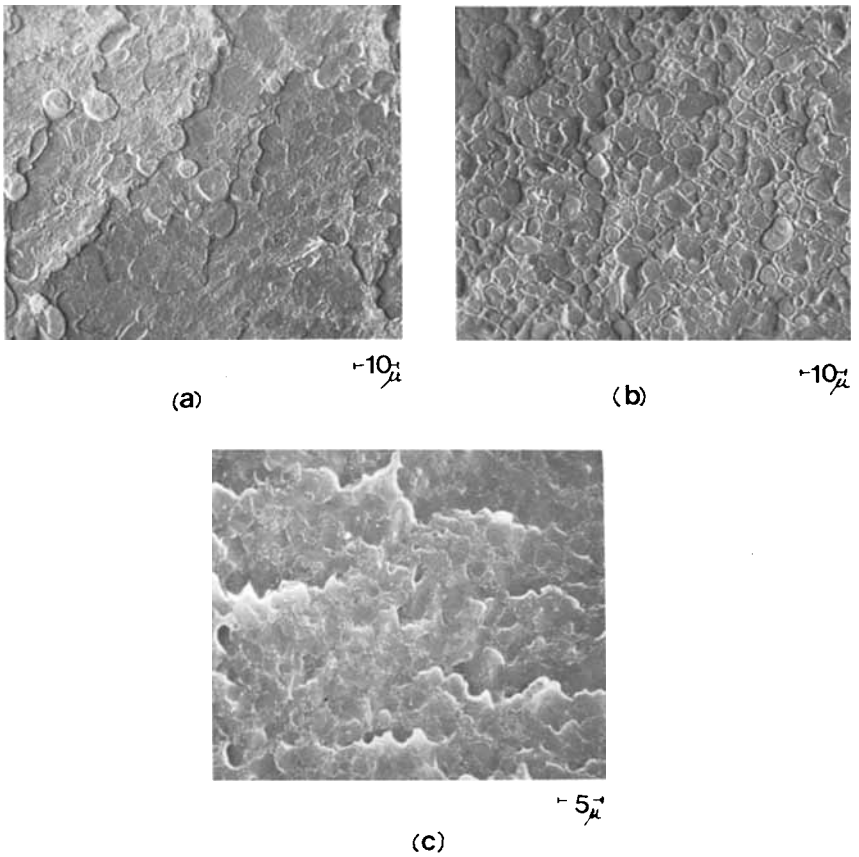

Fig. 7. SEM fracture surfaces of PE/PS 50/50 extrudates: (a) $\dot{\gamma} = 2.02\ s^{-1}$; (b) $\dot{\gamma} = 11.04\ s^{-1}$; (c) $\dot{\gamma} = 70.80\ s^{-1}$.

RHEOLOGICAL PROPERTIES OF COMPONENTS

Shear viscosity–shear rate data for the PS and HDPE melts at 180°C and 240°C are shown in Figure 1(a). The two melts have about the same viscosity at 180°C. However, the PS viscosity is much reduced at 240°C, while the PE experiences only a minor decrease. At low shear rates, the viscosity η is a constant, η_0, which decreases with increasing $\dot{\gamma}$.

Figure 1(b) contains a plot of principal normal stress difference N_1 as a function of shear stress. The N_1 values for the PE are larger than for the PS.

The transient elongational viscosity χ of the PS and PE at 180°C are shown in Figures 2(a) and 2(b). The PS data increases to a steady state value of $3\eta_0$ at low stretch rates. At higher stretch rates χ increases. The HDPE data generally do not exhibit a steady state. The elongations to break for the PS are significantly higher than the PE.

We now turn to the interpretation of this experimental data. In Figure 3, we plot η/η_0 vs. $\eta_0\dot{\gamma}$. η/η_0 falls off more rapidly with $\eta_0\dot{\gamma}$ for the PE than for the PS.

The temperature independence of plots of η/η_0 vs. $\eta_0\dot{\gamma}$ was first noted by Vinogradov and Malkin.[20] Similar η/η_0 plots for series of polyolefins with

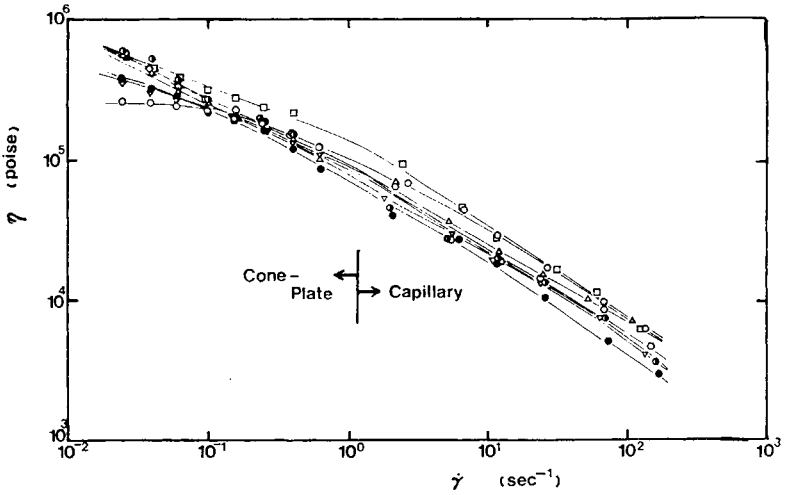

Fig. 8. Shear viscosity η of the PE/PS blends at 180°C as a function of shear rate: (●) PE; (▽) 90/10; (○) 70/30; (◑) 50/50; (△) 30/70; (□) 10/90; (○) PS.

varying molecular weight distributions have been published in earlier papers from our laboratories.[15,21] The broader the molecular weight distribution, the more rapidly η/η_0 decreases. Not dissimilar plots and results for polystyrene with varying molecular weight distributions have been given by others.[22]

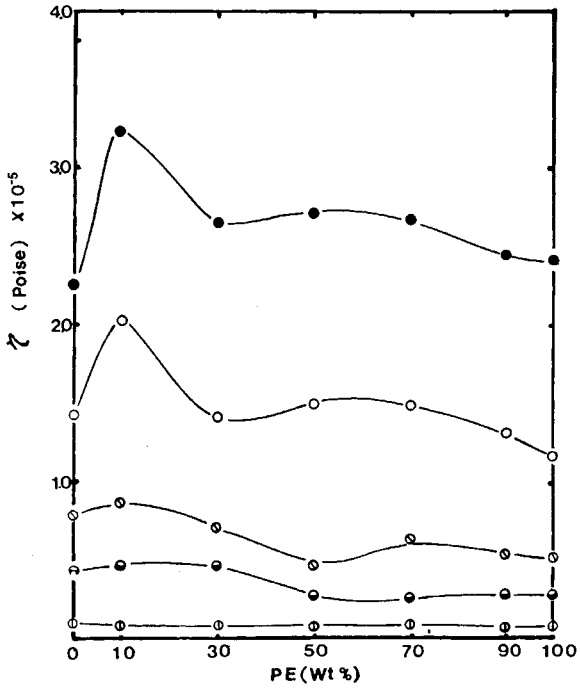

Fig. 9. Shear viscosity η of the PE (CX6109)/PS blends as a function of HDPE content at various shear rates (s^{-1}): (●) 0.1; (○) 0.4; (⊘) 1.92; (◒) 4.8; (⊖) 9.6.

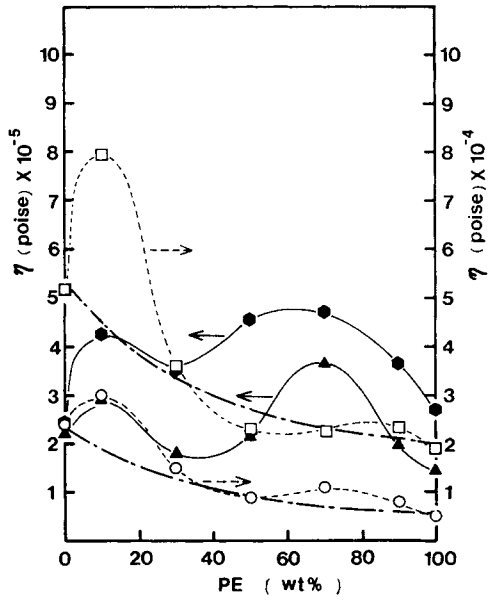

Fig. 10. Shear viscosity η of the PE/PS blends as a function of PE content at various shear stresses σ (dyn/cm^2) and comparison with Lees' equation (- · -): (●) 2.0×10^4; (▲) 4.0×10^4; (□) 2.0×10^5; (○) 4.0×10^5.

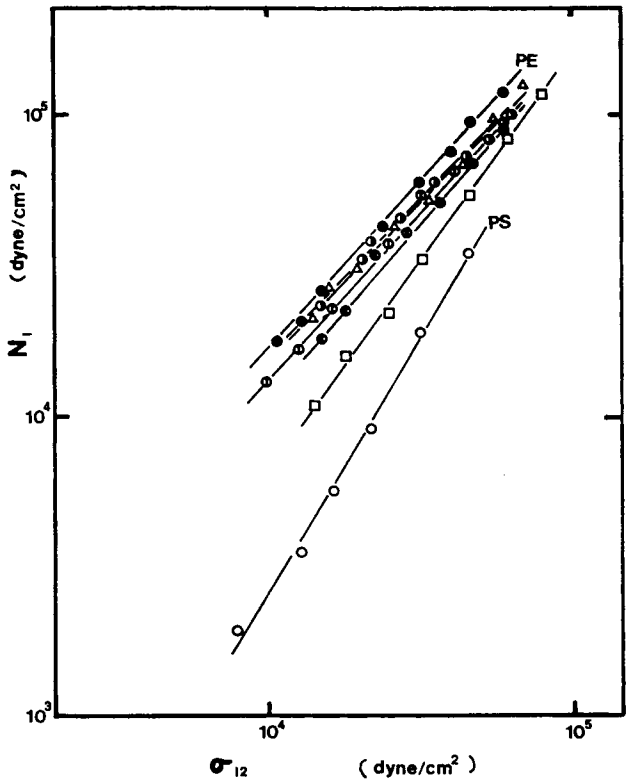

Fig. 11. Principal normal stress difference N_1 of the PE (CX6109)/PS blends as a function of shear stress: (●) PE; (◍) 90/10; (◐) 70/30; (◑) 50/50; (△) 30/70; (□) 10/90; (○) PS. T = 180°C.

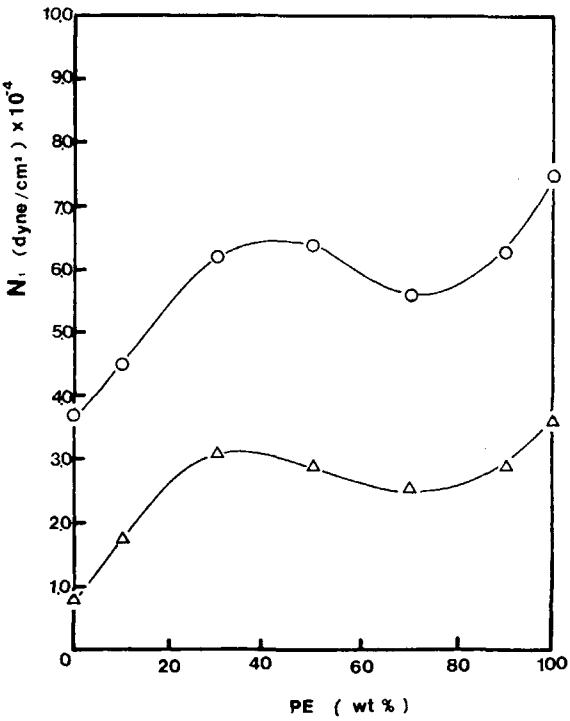

Fig. 12. Principal normal stress difference N_1 of the PE/PS blends as a function of composition at various shear stresses (dyn/cm^2): (○) 4.0×10^4; (△) 2.0×10^4.

Plots of N_1 vs. σ_{12} have been known since the work of Han[23] to be independent of temperature. Our data for N_1–σ_{12} are plots all similar to those published by Oda et al.[24] and later investigators.[15,21] These authors have concluded that the broader the molecular weight distribution, the higher N_1.

Our earlier investigations[15,21] of elongational flow of polymers of varying molecular weight distribution indicate that broad distribution filaments do not draw our uniformly filaments but develop necks and fail. Steady state elongational viscosities are only observed in narrower distribution samples as with our PS.

The η/η_0, N_1–σ_{12} and elongational flow results all indicate that PS and PE are largely linear polymers, with PS possessing a narrower molecular weight distribution.

PHASE MORPHOLOGY OF BLENDS FROM STATIC MIXER

Results. SEM photomicrographs of the blends from the static mixer are shown in Figures 4 and 5. The 90/10 through 70/30 and 30/70 through 10/90 exhibit a discrete morphology. The 50/50 composition is continuous. The dimensions of the discrete phases are generally of order 1–5 μm. We have computed number and weight average dimensions a_n and a_w:

$$a_n = \frac{\sum N_i a_i}{\sum N_i} \tag{7a}$$

$$a_w = \frac{\sum N_i a_i^2}{\sum N_i a_i} \tag{7b}$$

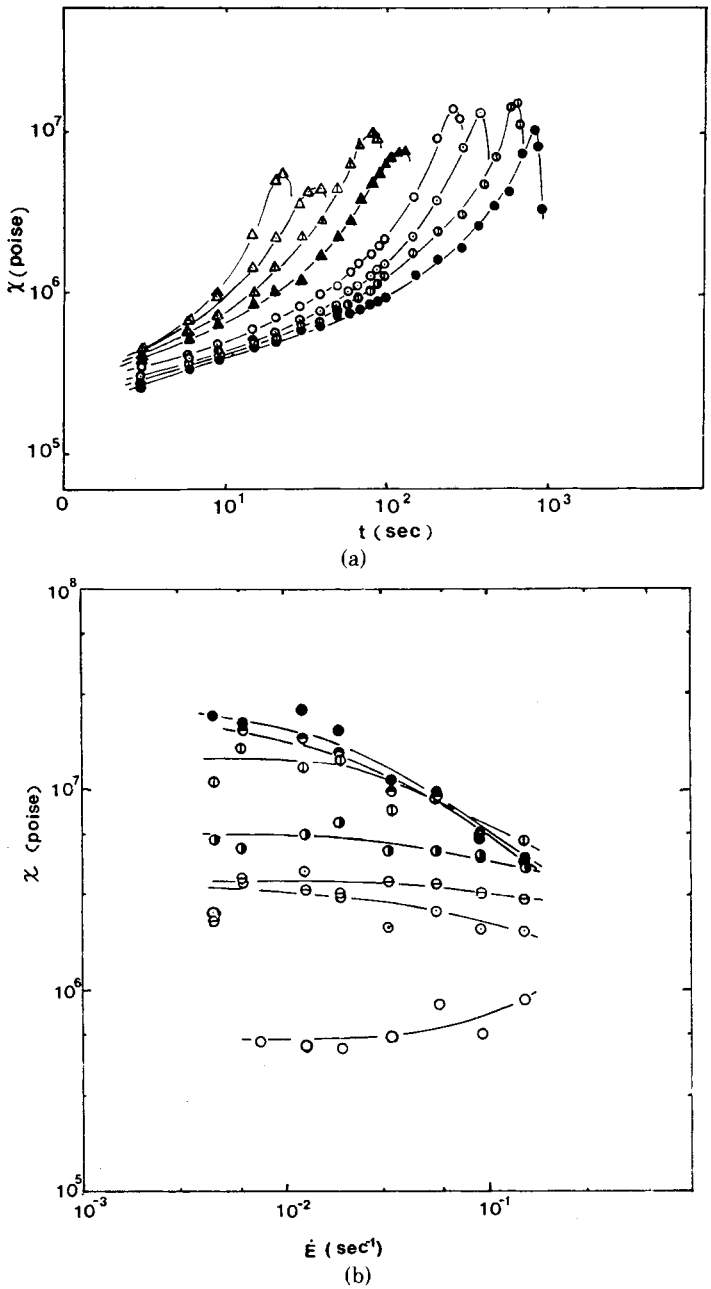

Fig. 13. (a) Transient elongational viscosity of PE (CX6109)/PS 50/50 blend; E (s^{-1}): (●) 4.46 × 10^{-3}; (◐) 7.14; (⊙) 1.22 × 10^{-2}; (○) 1.95; (▲) 3.31 (▲) 5.60; (▲) 9.10; (△) 1.50 × 10^{-1}. (b) Maximum elongational viscosity of PE (CX6109)/PS blends (180°C) of various compositions as a function of stretch rate: (●) PE; (◑) 90/10; (◒) 70/30; (◪) 50/50; (⊖) 30/70; (⊙) 10/90; (○) PS.

The numbers are summarized in Table I.

It may be seen that while increasing temperature the cross sections of the discrete islands become finer.

Discussion. Various earlier investigators notably Han and Kim[3] and Barentsen and Heikens[2] have investigated the detailed phase morphology of PE/PS

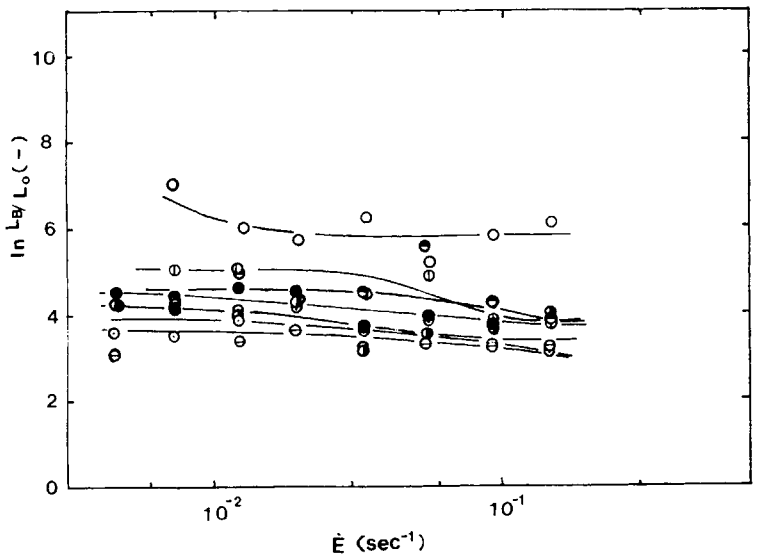

Fig. 14. Elongations to break of PE/PS blends (180°C) of varying composition as a function of stretch rate: (●) PE; (◑) 90/10; (◓) 70/30; (○) 50/50; (⊖) 30/70; (⊖) 10/90; (○) PS.

blends produced in various manners. Han et al. use a single screw extruder plus a Kenics Static Mixer while Heikens and his team use a single screw extruder. The phase morphologies are summarized in Table I. The sizes of the dispersed phase are quite similar.

The scale of phase morphology varies from blend system to blend system even if similar mixing conditions are used. Studies by Liang et al.[25] in our laboratories indicate that with the polypropylene/nylon-6 system mixed with the same static mixer (at 230°C) the sizes of the disperse phase are an order of magnitude larger than what we have found here.

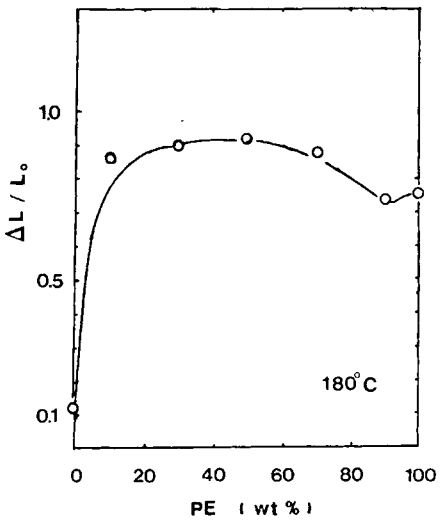

Fig. 15. Shrinkage of PE (CX6109)/PS blends as a function of composition.

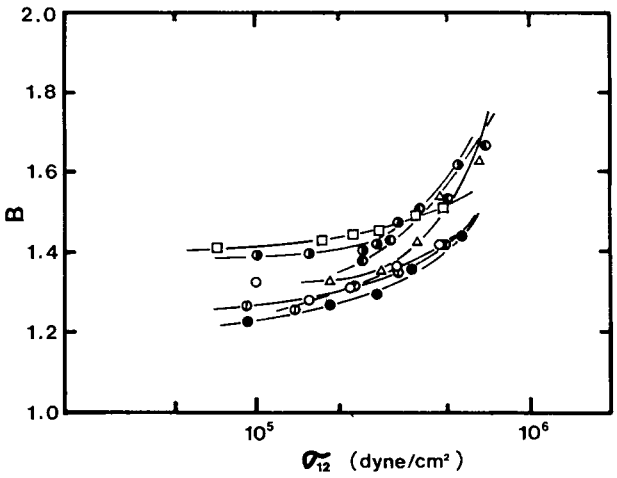

Fig. 16. Extrudate swell of PE/PS blends as a function of die wall shear stress: (□) PE; (○) 90/10; (●) 70/30; (○) 50/50; (◑) 30/70; (◐) 10/90; (△) PS. L/D = 40; D = 0.058 (in.).

MORPHOLOGIES OF BLENDS IN RHEOMETERS

Results. The blend systems sheared in the gap between the cone and plate in the Mechanical Spectrometer and the extrudates emerging from the capillary have been cross-sectioned and the fracture surfaces analyzed. The studies were carried out at 180°C.

Typical cross sections for fracture surfaces for the samples removed from the cone-plate geometry are shown in Figure 6. These show ellipsoidal filaments of the dispersed phase embedded in a continuous matrix for the 90/10, 70/30, 30/70, and 10/90 compositions. The filaments point in the direction of flow, i.e., the circumferential direction. Diameters of the filaments are summarized in Table II.

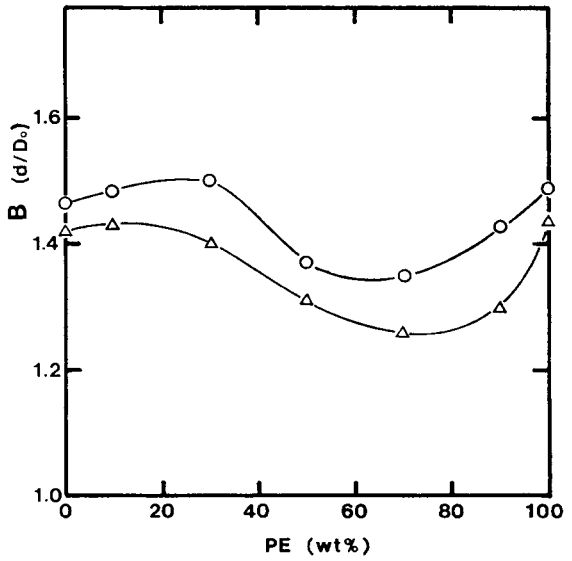

Fig. 17. Extrudate swell of PE/PS blends as a function of composition; σ_w (dyn/cm²): (○) 0.40 × 10^6; (△) 0.20 × 10^6. L/D = 40; D = 0.058 (in.).

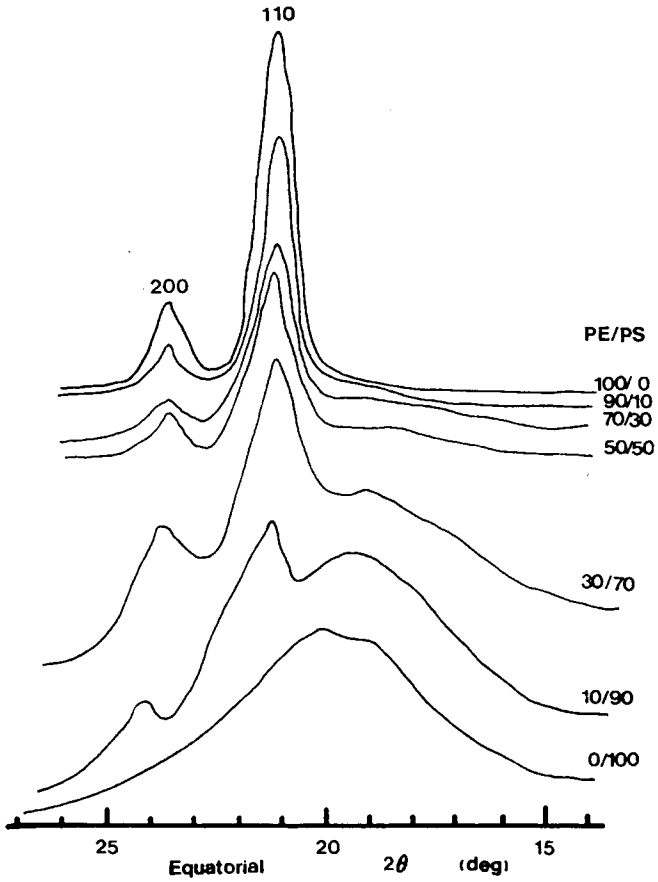

Fig. 18. Diffractometer scans for PE/PS blends.

Fracture surface cross sections of extrudates are shown in Figure 7. The minor components are ligaments with their major axes along the axis of the capillary. Diameters are summarized in Table III.

Discussion. In the rheometers as in the extrudates from the static mixer, the morphology is finely dispersed with dimensions generally of order 1–5 μm. This compares to apparatus dimensions of order 1500 μm. As the deformation rates increase, there is some tendency for the dispersed phase ellipsoidal ligaments to increase in aspect ratio and decrease in diameter.

Earlier investigators of the PE/PS blends have not looked at the influence of flow in rheometers on phase morphology. A similar study for polypropylene (PP)/nylon 6 has been given by Liang et al.[25] from our own laboratories. Their results are in striking contrast to ours. They observed that the size of the polypropylene islands dispersed in a nylon 6 sea grew with time in a quiescent system, but are sharply reduced with deformation rate.

Liang et al.[25] hypothesize that the coarseness of the morphology depends upon the dimensionless group $\kappa/\eta\dot{\gamma}a$, where κ is the interfacial tension, η the continuous phase viscosity, and $\dot{\gamma}$ the shear rate. The PP/nylon-6 system has a higher interfacial tension and thus a larger discrete phase size, a. The lower value of κ the interfacial tension and higher η for the PE/PS system lead to a finer morphology.

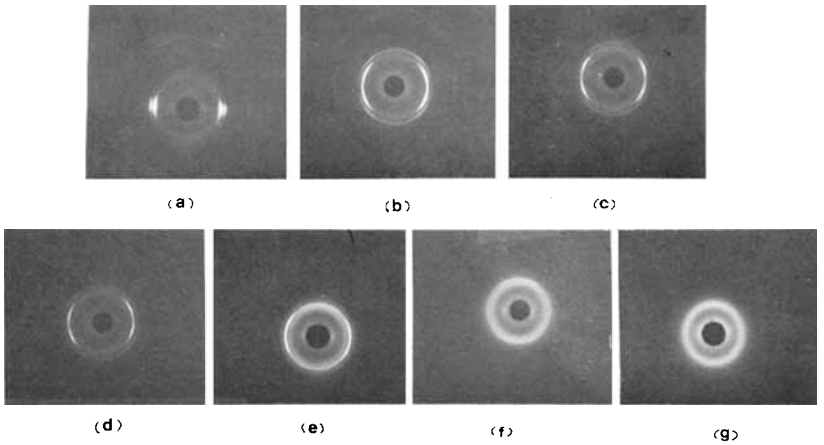

Fig. 19. WAXS patterns of melt spun fibers: (a) PE 100; (b) PE 90/PS 10; (c) PE 70/PS 30; (d) PE 50/PS 50 (V_L/V_0 = 215); (e) PE 30/PS 70; (f) PE 10/PS 90; (g) PE 100.

RHEOLOGICAL PROPERTIES OF BLENDS

Shear Viscosity. The steady shear viscosity of the PE/PS blends is shown as a function of shear rate at 180°C in Figure 8. The data from the cone plate and capillary instruments is consistent. The viscosity is plotted as a function of composition at fixed shear rates in Figure 9 and at various shear stresses in Figure 10. The viscosity exhibits a minimum and a maximum in both figures.

Principal Normal Stress Difference. The principal normal stress difference of the PE/PS blends is shown as function of shear stress in Figure 11. N_1 is plotted as a function of composition in Figures 12 at constant shear stress. The plots exhibit a maximum of 30% PE and a minimum at 70%.

Elongational Flow. A typical transient elongational viscosity χ plot for a 50/50 blend at various extension rates is shown in Figure 13(a). It is not possible to achieve steady state elongational viscosity in the blend systems. Figure 13(b) shows "maximum" elongational viscosity as a function of stretch rate. The elongation to break of the filaments is shown in Figure 14 as a function of extension rate. It is found that even small additions of the PE to the PS make substantial changes in the rheological properties. The elongations to break of the PS are reduced more than order of magnitude at even 10% PE.

Discussion. The continuity of the shear viscosity–shear rate plots for the blend systems indicate that data from both instruments are consistent. This is perhaps not unreasonable with the small scale of the dispersion relative to the instrument dimensions.

The viscosity–composition plots exhibit minima and maxima at low deformation rates but become monotonic at higher shear rates. This type of complexity of viscosity composition plots is common in the literature.[1,3,25] Two theories of the viscosity of two phase liquids are worthy of attention. Taylor[26] considered the hydrodynamics of a *dilute* suspension of spheres a liquid B dispersed in a liquid A. Taylor showed that the shear viscosity of the two phase system to the first order is

$$\eta = \eta_A \left[1 + 2.5 \left(\frac{1 + \frac{2}{5}\,\eta_A/\eta_B}{1 + \eta_A/\eta_B}\right) \phi_B\right] \tag{8}$$

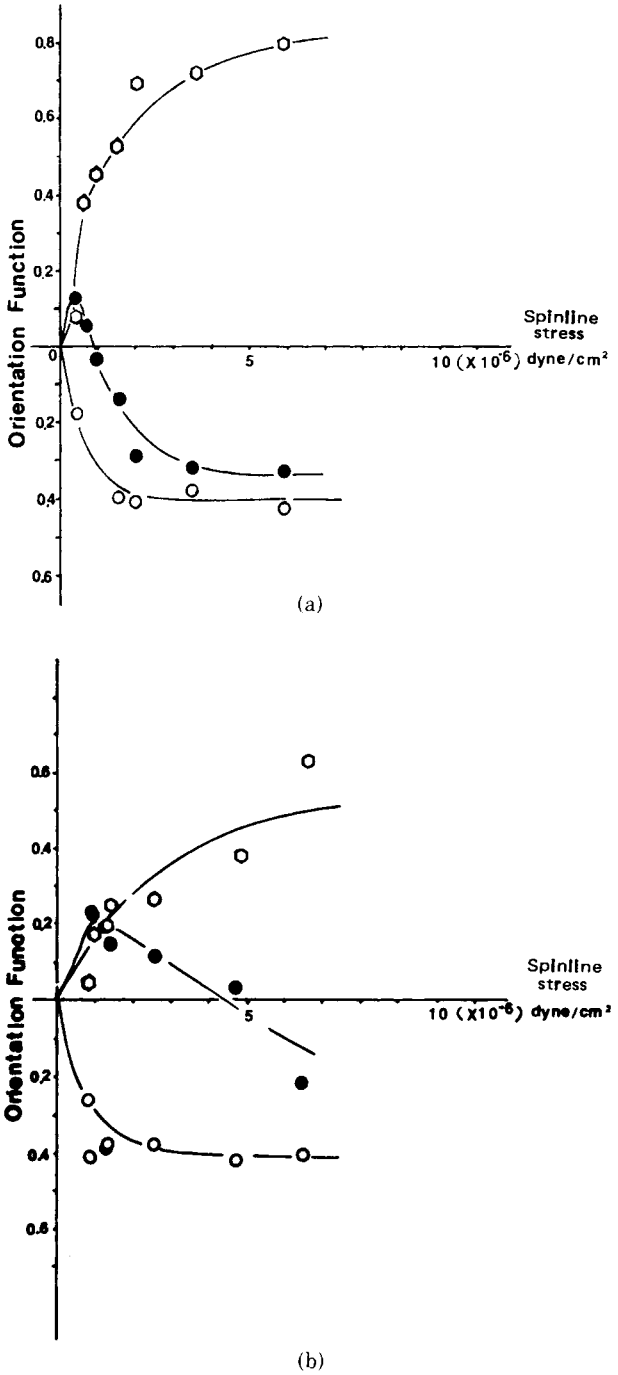

Fig. 20. Hermans-Stein orientation factors f_a (●), f_b (○), f_c (○) for crystalline phase of HDPE (CX6109) in blends as a result of spinline stress: (a) 100/0; (b) 90/10; (c) 70/30; (d) 50/50; (e) 30/70; (f) 10/90.

The shear viscosity is always increased by the presence of the second spherical droplet even if it is lower in viscosity.

A second and simpler theory is that of Lees.[27] In this model one considers

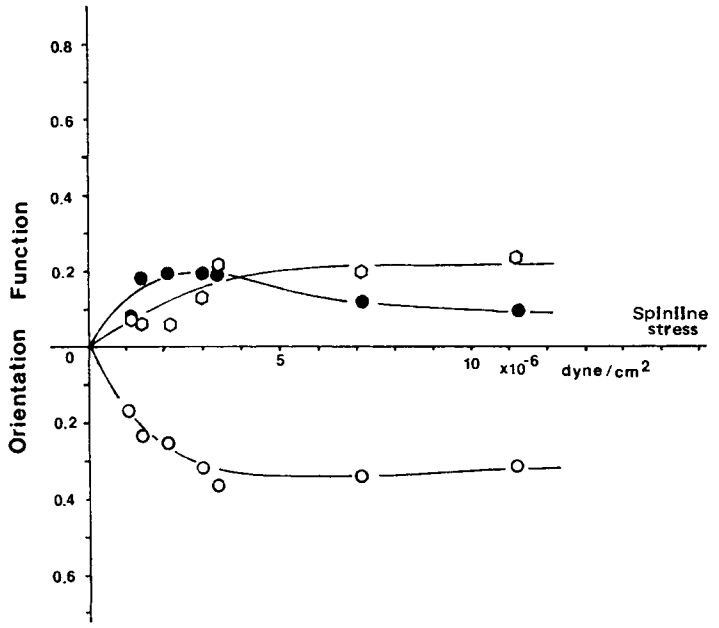

(c)

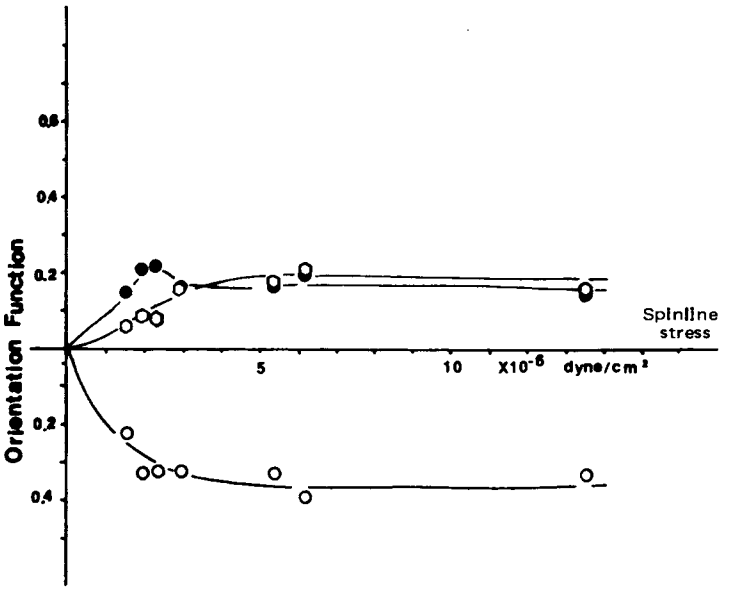

(d)

Fig. 20 (*Continued from the previous page.*)

a series of parallel layers (or ligaments and matrix) in a region of constant shear stress σ_{12}. The mean shear rate for phases A and B is

$$\bar{\dot{\gamma}} = \phi_A \dot{\gamma}_A + \phi_B \dot{\gamma}_B \tag{9}$$

Expressing the local shear rate $\dot{\gamma}_j$ as the ratio of shear stress σ_{12} to viscosity η_j and $\dot{\gamma}$ as the ratio of σ_{12} to average system viscosity η yields the result of less:

$$1/\eta = \phi_A/\eta_A + \phi_B/\eta_B \tag{10}$$

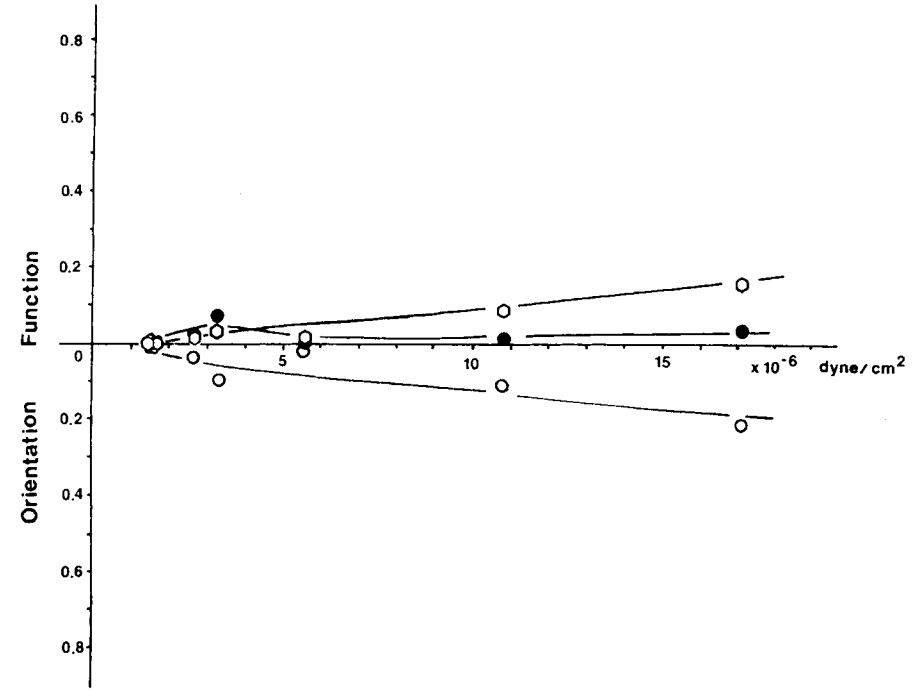

(e)

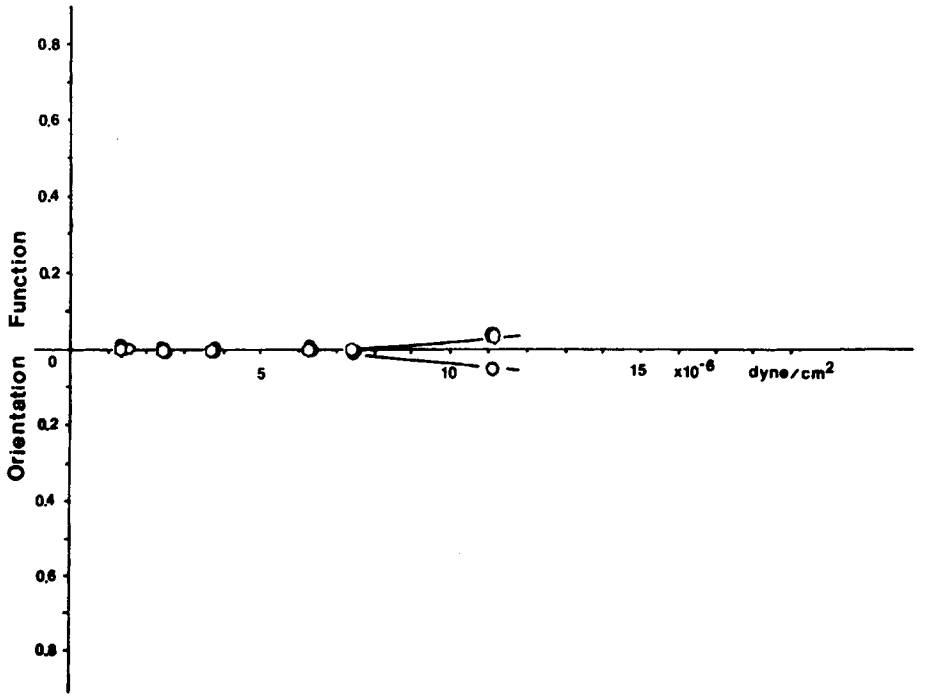

(f)

Fig. 20 (*Continued from the previous page.*)

It is obviously a theory for higher concentrations than eq. (8). Equation (10) was first applied to polymer melts in the 1960s.[28,29] In Figure 10, we compare eq. (10) with our experimental data. The predictions of eq. (10) are generally

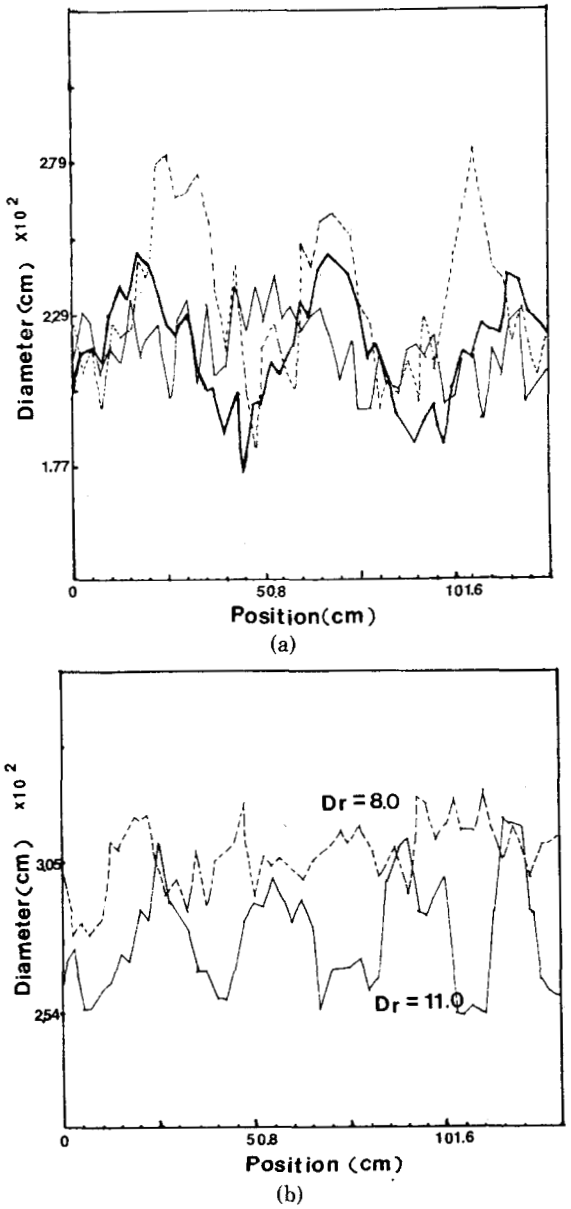

Fig. 21. Diameter fluctuations (180°C) in PE/PS blend fibers. (a) (—) PE (CX6109); (- - -) 50/50; (—) PS. (b) 50/50.

below the experimental data points with the differences being lowest at the highest shear stresses.

An explanation for the "dog-eared" discosity–composition plots of Figure 10 can be developed by considering eq. (8) to be valid at low levels of component A or B. This predicts a viscosity which increases the concentration of the second component. At intermediate compositions a cocontinuous phase structure develops in which eq. (10) is valid. This results in the sharp drop in viscosity in this region.

The principal normal stress difference and elongational viscosity behavior indicates that addition of small amounts of PE makes substantial changes in the

TABLE IV
Melt Spinning Instabilities for PE/PS Blends

PS/PE composition	Onset of draw resonance
0/100	20
10/90	5.0
30/70	9.0
50/50	10.5
70/30	11.0
90/10	13.0
100/0	15.0

PS. Generally the trend of N_1 at fixed shear stress with composition is opposite to the viscosity. One can envisage these changes as being due to long continuous elastic filaments of PE in the PS matrix. The elongational failure characteristics also suggest a weakest link perspective. Blends will show ductile failure which is initiated in the PE component.

EXTRUDATE CHARACTERISTICS

Extrudate Shrinkage. The PE shows substantially greater shrinkage than the PS. The behavior of the blends is shown in Figure 15. Small amounts of PE produce greatly enhanced shrinkage. In some cases the PE/PS blends show even greater shrinkage than the pure PE.

Extrudate Swell. The extrudate swell of the blends are plotted as a function of the shear stress in Figure 16. The data is replotted as a function of composition in Figure 6. It may be seen that that data exhibits a maximum and a minimum in the composition plots.

Fig. 22. Extracted 10/90 PE/PS blend fibers, draw ratio, $V_L/V_0 = 75.4$, spinline stress, $\sigma = 3.7 \times 10^6$ dyn/cm^2.

TABLE V
Diameters of Minifibers

PE/PS composition	1	d_L (μm) at various V_L/V_0 18.8	37.6	56.6	75.4
PE 90/PS10	1.47	1.05	0.50	0.38	0.22
70/30	3.18	1.16	0.90	0.34	0.42
50/50	2.72	1.35	0.98	0.60	—
30/70	1.48	—	0.63	—	—
10/90	0.75	—	0.43	0.35	—

The maxima in extrudate swell are found to correspond to maxima in principal normal stress differences or normal stress–shear ratios, N_1/σ_{12}, as indicated in Figure 12. This is the expected theories of swell such as that of Tanner[30] (see also Huang and White[31]) if this is applied to blend systems.

MELT SPINNING

Structure Development. Filaments were melt spun both through air and through an isothermal chamber into a quench bath and then taken up. The crystalline orientation in the PE phase was given primary attention. Diffractometer scans for PE/PS blends are shown in Figure 18 and WAXS film patterns in Figure 19. The decrease in PE orientation is obvious and may best be seen from the 200 reflections which shift from equatorial to meridional as PS contact increases. Hermans–Stein orientation factors for the HDPE crystalline regions were computed using eqs. (4) and (5) and are plotted in Figure 20 as a function of spinline stress. At any stress the c-axis and b-axis orientation factors decrease. f_a tends from zero to positive to negative.

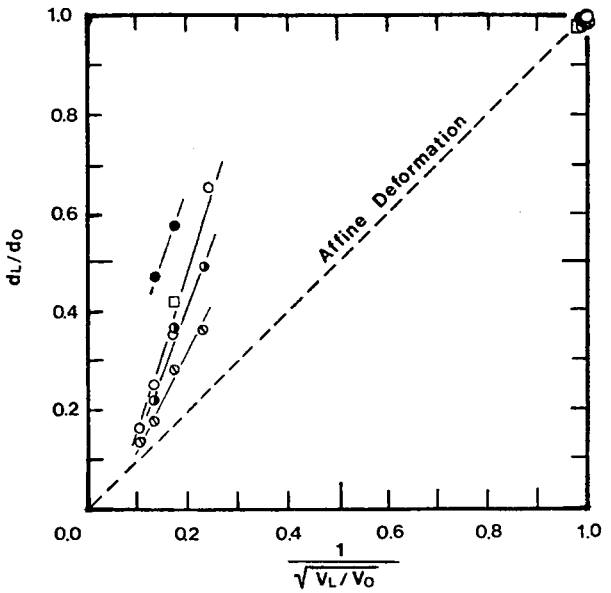

Fig. 23. Diameters of minifibers as a function of draw ratio V_L/V_0; PE/PS: (○) 90/10; (◔) 70/30; (◑) 50/50; (□) 30/70; (●) 10/90.

It is well established for both polyethylene and polypropylene that the crystalline orientation factors and morphology of melt spun fibers correlate with spinline stress.[32,33] The decrease of the orientation factors with addition of PS is quite striking and contrasts with studies of the variation of crystalline orientation by Liang et al.[25] and Shimomura et al.[34] in our laboratories. Liang et al. melt-spun polypropylene/nylon 6. They found that the crystalline orientation of polypropylene as determined by WAXS is independent of nylon-6 content at the same stress. This is in sharp contrast to the behavior of Figure 20. Similar behavior to the results of Liang et al. have been reported by Shimomura et al., who made tubular film from polyethylene/polypropylene.

A possible reason for this behavior is the strong dependence of the viscosity of PS on temperature relative to that of PE. The stress exerted on the two phases in the spinline may significantly redistribute itself in this case becoming higher in the more viscous PS and lower in PE. Low orientation results in the PE melt and eventually crystalline phase.

Spinline Disturbance and Instability. The melt spun filaments exhibit nonuniform diameters throughout the range of spinning conditions. Typical diameter fluctuations are shown in Figure 21. At a critical drawdown ratio the periodicity becomes regular.

The critical draw ratio producing this high amplitude oscillation is shown in Table IV. It is seen that the critical draw ratio exhibits a minimum when considered as a function of composition.

The minimum exhibited to the critical drawdown ratio required to achieve draw resonance is not an unexpected result. The nonuniformity of the local rheological properties in a blend system would be expected to make it more susceptible to disturbances in elongational flow. This is indeed what was observed in simple elongational flow stretching experiments summarized in Figure 14. Generally draw resonance corresponds to ductile failure in simple elongational flow as has been noted in earlier papers from our laboratories.[17,35] Blending the PE into PS has an effect analogous to broadening the molecular weight distribution, though the mechanism is different.

MINIFIBERS

Results. PE/PS blend fibers were melt-spun through air under conditions where no draw resonance was observed. The melt spun fibers were then extracted with toluene. The products resulting from this extraction ranged from extremely small diameter fibers at high PS levels to porous PE filaments. The former are of more interest to us and are shown in Figure 22. Diameters of mini fibers are summarized in Table V.

As the level of drawdown increases the minifiber diameters decrease in diameter. At a draw ratio V_L/V_0 of unity they are an average of 0.75 μm. When the draw ratio is increased they are reduced to 0.35 μ at V_L/V_0 of 56.6. This trend is shown in Figure 23. The data of Figure 23 indicate that the drawdown in diameter occurs in general more slowly than one would expect from affine deformations. This form of this figure derives from the balance

$$\frac{\pi d_0^2}{4} V_0 = \frac{\pi d_L^2}{4} V_L \tag{11}$$

where we have replaced the a used for dispersed flow in contained geometries with d. This may be rearranged to give

$$\frac{d_L}{d_0} = \frac{1}{\sqrt{V_L/V_0}} \tag{12}$$

This suggests that the dispersed ligaments periodically break and recover, rather than being drawdown in an affine manner.

CONCLUSIONS

A broad based study of the development of phase morphology, molecular orientation, rheological behavior, and processing of a high density polyethylene/polystyrene (PE/PS) blend system has been reported. This continues earlier studies of blend systems in our laboratories which have in recent years included polypropylene/nylon 6[25] and polyethylene/polypropylene.[34] Certain trends are clear.

(i) The phase morphologies developed by screw extruder/static mixer system generally involve phase dimensions of 1–5 μm except at 50/50 loadings where dimensions up to 10 μm are obtained. Some reduction is obtained by subsequent shearing in viscometric instruments. Phase dimensions as fine as 0.6 μm are obtained in a 10/90 PE/PS at higher shear rates in a capillary die. These diameters may be reduced even further by melt spinning. Small diameter minifibers may be produced by extracting the PS (with toluene). Minifibers of diameter of order 0.2 μm may be produced. The morphologies are much finer than we have found in earlier studies of the polypropylene/nylon 6 system.[25] This is presumably because of the lower interfacial tensions.

(ii) The crystalline polyethylene orientation developed in melt-spun PE/PS fibers is significantly reduced by the presence of polystyrene when comparisons are at the same spinline stress. This differs from observations made earlier on polypropylene/nylon 6[25] and polyethylene/polypropylene[34] blends, where crystalline orientation in the polyethylene and polypropylene phases depend on the process stress in a manner equivalent to the pure phases. This is attributed to the greater temperature dependence of the viscosity of the PS on which the stress increasingly concentrates as the melt blends descends the threadline.

(iii) The shear viscosity and principal normal stress difference depend on the volume fractions of the individual polymers in a complex manner. Maxima and minima are observed as a function of composition. Interpretations of the shear viscosity are offered in terms of using Taylor's theory of emulsions[26] for dilute phases and Lees' theory of lamellae flow[27] for intermediate concentrations.

(iv) Addition of PE to PS substantially increases the shrinkage of extrudates.

(v) The extrudate swell of the blends correlates with the principal normal stress difference N_1 and its ratio to the shear stress.

(vi) The uniaxial elongational flow and melt spinning characteristics of the blends are dominated by the high density polyethylene. Addition of PE significantly reduces the elongation to break and makes the spinline unstable. This may in good part be due to nonhomogeneity and/or "weakest link" behavior.

This research was supported in part by the Polymers Program of the Division of Materials of the National Science Foundation under NSF Grant DMR-80-26051.

References

1. C. D. Han and T. C. Yu, *J. Appl. Polym. Sci.*, **15,** 1163 (1971).
2. W. M. Barensten and D. Heikens, *Polymer*, **14,** 579 (1973).
3. C. D. Han and Y. W. Kim, *Trans. Soc. Rheol.*, **19,** 245 (1975).
4. B. L. Lee and J. L. White, *Trans. Soc. Rheol.*, **19,** 481 (1975).
5. J. R. Stell, D. R. Paul and J. W. Barlow, *Polym. Eng. Sci.*, **16,** 496 (1976).
6. A. Aref-Azar, J. N. Hay, B. J. Marsden, and N. Walker, *J. Polym. Sci., Polym. Phys. Ed.*, **18,** 637 (1980).
7. C. E. Locke and D. R. Paul, *J. Appl. Polym. Sci.*, **17,** 2791 (1973).
8. W. M. Barentsen, W. Heikens, and P. Piet, *Polymer* **15,** 119 (1974).
9. D. Heikens and W. Barentsen, *Polymer*, **17,** 69 (1977).
10. D. Heikens, N. Hoen, W. Barentsen, P. Piet, and H. Ladan, *J. Polym. Sci., Polym. Symp.*, **62,** 309 (1978).
11. C. R. Lindsey, D. R. Paul, and J. W. Balrow, *J. Appl. Polym. Sci.*, **8,** 1 (1981).
12. K. Walters, *Rheometry*, Chapman and Hall, London, 1977.
13. J. L. White, in *Rheometry: Industrial Applications*, K. Walters, Ed., Wiley, New York, 1980.
14. Y. Ide and J. L. White, *J. Appl. Polym. Sci.*, **22,** 1061 (1978).
15. H. Yamane and J. L. White, *Polym. Eng. Rev.*, **2,** 167 (1983).
16. Y. Suetsugu and J. L. White, *J. Appl. Polym. Sci.*, **28,** 1481 (1983).
17. W. Minoshima, J. L. White, and J. E. Spruiell, *J. Appl. Polym. Sci.*, **25,** 287 (1980).
18. C. W. Bunn, *Trans. Faraday Soc.*, **35,** 482 (1939).
19. R. S. Stein, *J. Polym. Sci.*, **31,** 327 (1958).
20. G. V. Vinogradov and A. Y. Malkin, *J. Polym. Sci.*, **4,** 135 (1966).
21. W. Minoshima, J. L. White, and J. E. Spruiell, *Polym. Eng. Sci.*, **20,** 1166 (1980).
22. S. Onogi, T. Masuda, I. Shiga, and F. M. Costachuk, *Appl. Polym. Symp.*, **20,** 37 (1973).
23. C. D. Han, *Polym. Eng. Sci.*, **11,** 205 (1971).
24. K. Oda, J. L. White, and E. S. Clark, *Polym. Eng. Sci.*, **18,** 25 (1978).
25. B. Liang, J. L. White, J. E. Spruiell, and B. C. Goswami, *J. Appl. Polym. Sci.*, **28,** 2011 (1983).
26. G. I. Taylor, *Proc. Roy. Soc.*, **A138,** 431 (1932).
27. C. Lees, *Proc. Phys. Soc.*, **17,** 460 (1900).
28. R. F. Heitmiller, R. Z. Naar, and H. H. Zabusky, *J. Appl. Polym. Sci.*, **8,** 873 (1964).
29. K. Hayashida, J. Takahashi, and M. Matsui, *Proc. 5th Int. Rheol. Cong.* **4,** 525 (1970).
30. R. I. Tanner, *J. Polym. Sci., A-2* **8,** 2067 (1970).
31. D. C. Huang and J. L. White, *Polym. Eng. Sci.*, **19,** 609 (1979).
32. J. R. Dees and J. E. Spruiell, *J. Appl. Polym. Sci.*, **18,** 1053 (1974).
33. H. P. Nadella, H. M. Henson, J. E. Spruiell, and J. L. White, *J. Appl. Polym. Sci.*, **21,** 3003 (1977).
34. Y. Shimomura, J. E. Spruiell, and J. L. White, *Polym. Eng. Rev.*, **2,** 417 (1983).
35. J. L. White and Y. Ide, *J. Appl. Polym. Sci.*, **22,** 3057 (1978).

Received August 19, 1983
Accepted December 1, 1983